© 2019. Published by The Company of Biologists Ltd | Journal of Experimental Biology (2019) 222, jeb207787. doi:10.1242/jeb.207787

METHODS & TECHNIQUES

Controlling and measuring dynamic odorant stimuli in the laboratory

Srinivas Gorur-Shandilya[1,2,*], Carlotta Martelli[2,3,‡], Mahmut Demir[2] and Thierry Emonet[1,2,4,§]

ABSTRACT

Animals experience complex odorant stimuli that vary widely in composition, intensity and temporal properties. However, stimuli used to study olfaction in the laboratory are much simpler. This mismatch arises from the challenges in measuring and controlling them precisely and accurately. Even simple pulses can have diverse kinetics that depend on their molecular identity. Here, we introduce a model that describes how stimulus kinetics depend on the molecular identity of the odorant and the geometry of the delivery system. We describe methods to deliver dynamic odorant stimuli of several types, including broadly distributed stimuli that reproduce some of the statistics of naturalistic plumes, in a reproducible and precise manner. Finally, we introduce a method to calibrate a photo-ionization detector to any odorant it can detect, using no additional components. Our approaches are affordable and flexible and can be used to advance our understanding of how olfactory neurons encode real-world odor signals.

KEY WORDS: Mass flow controller, Photo-ionization detector, Automation, Calibration, Odor control, Olfaction

INTRODUCTION

The study of sensory systems requires precise control and measurement of stimuli. The ease of generation and measurement of light and sound stimuli have led to a detailed understanding of how primary visual and auditory neurons encode visual and auditory stimuli (Hudspeth, 2014; de Ruyter van Steveninck and Bialek, 1988; Smirnakis et al., 1997; Laughlin, 1989). Olfactory stimuli are harder to generate and measure because they consist of small molecules of bewildering variety that have to be transported from the source to olfactory receptor neurons (ORNs) on sensory organs. The kinetics of odor stimuli depend on physical and chemical parameters (Andersson et al., 2012; Martelli et al., 2013). Far from surfaces, odors are transported by advection and diffusion, which depend linearly on odor concentration. Thus, changing the concentration of odor at the source merely scales the resulting stimulus. If interactions with surfaces could be avoided completely, odor pulses of different amplitudes could in principle be delivered with exactly the same kinetics. Thus, normalizing stimuli of the same odor but different concentration by their maximum intensity would collapse them on the same curve (Andersson et al., 2012).

In practice, odor molecules can diffuse through the airstream onto surfaces. Binding to surfaces is a nonlinear process because it depends on the concentration of odor in the gas phase and that of odor molecules already bound to the surface. Thus, surface interactions break the linearity of odor transport, which renders the kinetics of odor transport concentration dependent (see Materials and Methods). Natural odors can consist of multiple odorants with different surface affinities. Surface interactions might affect some components of an odor more than others, possibly breaking the coherence of an odor signal. These interactions can significantly alter the kinetics of identically delivered stimuli, complicating the analysis of ORN responses (Martelli et al., 2013; Su et al., 2011). Surface-odorant interactions are significant both in laboratory conditions used for physiology and behavior (Gershow et al., 2012; Hernandez-Nunez et al., 2015; Mathew et al., 2013; Klein et al., 2017; Budick and Dickinson, 2006; Frye and Dickinson, 2004; Fishilevich et al., 2005; Gaudry et al., 2013), and in real-world scenarios (Riffell et al., 2009, 2008; Murlis et al., 1992, 2000; Murlis and Jones, 1981).

Here, we describe simple approaches to make odorant stimuli delivery more controllable and reproducible. We first analyze the properties of a standard odor delivery system using a simple mathematical model. We provide some intuition about why the output of the delivery system may not match expectations. Previous work has used either simple odor delivery systems that can generate simple stimuli or custom-designed instruments capable of complex stimuli but that are challenging to engineer (Martelli et al., 2013; Hallem and Carlson, 2006; Nagel and Wilson, 2011; Kim et al., 2011; Cafaro, 2016). There is a growing interest in connecting neural activity to behavior (Gershow et al., 2012; Kato et al., 2014; Hernandez-Nunez et al., 2015; Gepner et al., 2015; Davies et al., 2015; Gomez-Marin et al., 2011; Thoma et al., 2014) and therefore an increasing need for studying the neural response to naturalistic stimuli. We describe methods to deliver complex and intermittent odorant stimuli using off-the-shelf components and show how the same delivery system can be used to reproducibly generate an odorant stimulus that mimics the statistics of natural stimuli. Finally, we describe a novel approach to calibrate a photo-ionization detector (PID) to any odorant it can detect, to enable quantitative comparisons of stimuli across time and across different laboratories.

MATERIALS AND METHODS

Mathematical model of a simple delivery system

We consider a delivery system schematized in Fig. 1A. Clean air is injected at the constant flow rate Q_2 inside a cylindrical odor delivery tube of inner radius R_2. From a lateral hole a secondary air stream carrying odor at gas phase concentration c_1 is injected with flow rate Q_1 under control of a solenoid valve placed upstream of the odor source.

[1]Interdepartmental Neuroscience Program, Yale University, New Haven, CT 06511, USA. [2]Department of Molecular, Cellular, and Developmental Biology, Yale University, New Haven, CT 06511, USA. [3]Department of Biology, University of Konstanz, Konstanz 78457, Germany. [4]Department of Physics, Yale University, New Haven, CT 06511, USA.
*Present address: Volen Center for Complex Systems, Brandeis University, Waltham, MA 02453, USA. ‡Present address: Institute of Developmental Biology and Neurobiology (iDN), Johannes Gutenberg University Mainz, 55128 Mainz, Germany.

§Author for correspondence (thierry.emonet@yale.edu)

S.G.-S., 0000-0002-7429-457X; C.M., 0000-0002-5663-6580; M.D., 0000-0002-3278-7843; T.E., 0000-0002-6746-6564

Received 24 May 2019; Accepted 24 October 2019

Journal of Experimental Biology (2019) 222, jeb207787. doi:10.1242/jeb.207787

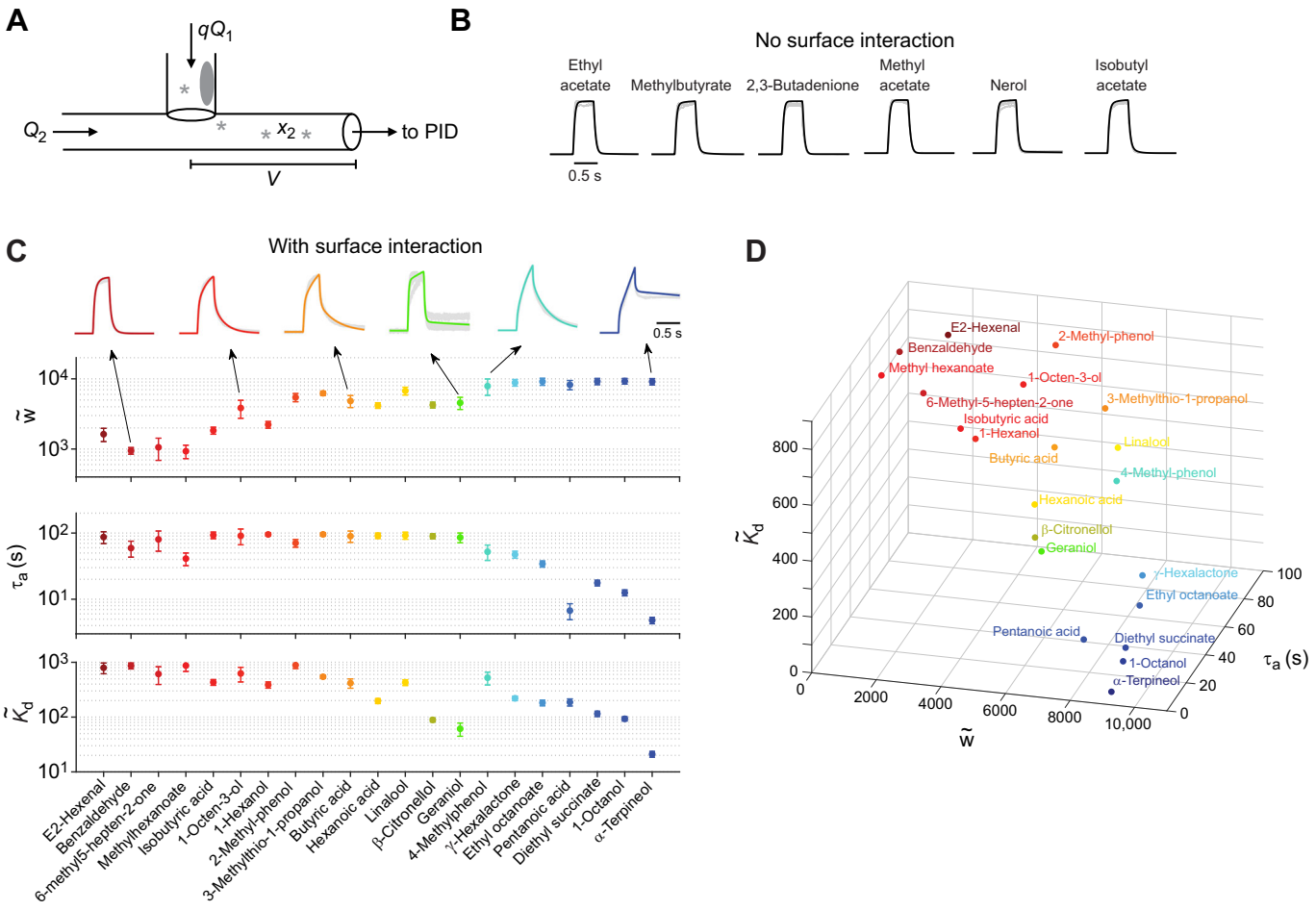

Fig. 1. A simple model reproduces the diversity of odorant pulse kinetics. (A) Schematic diagram of an odor delivery system. Air flows in the odor chamber with flow rate Q_1 controlled by a solenoid valve (q). The odorous stream enters the main delivery tube where clean air flows with rate Q_2. x_2 is the normalized concentration of odor in gas phase within the volume V (Eqn 7). A photoionization detector (PID) is used to measure the amount of odor exiting the tube. (B) Normalized photo-ionization detector (PID) recordings (gray) and model predictions (black) for six odors for which surface interactions are negligible. (C,D) Parameters of model fitted to PID measurements of 21 odorants for which surface interaction cannot be neglected. Error bars show standard deviation estimated from 30 fits. Colored traces in C show model predictions. $\tilde{w}$, density of odor binding sites on the inner surface of the tube; τ_a, time scale of odor to surface binding; $\tilde{K}_d$, dissociation constant between the odor and surface.

In the absence of interactions between odorant molecules and surfaces, the gas phase concentration of odor inside the delivery tube, c_2, obeys the equation:

$$\tau_2 \frac{dc_2}{dt} = \underbrace{q\phi c_1}_{\text{influx}} - \underbrace{(1-q\phi)c_2}_{\text{efflux}}. \quad (1)$$

The first and second terms on the right represent the odor that comes in and out of the delivery tube, respectively. $\tau_2 = V_2/Q_2$ is the time it takes to replace all the air in the delivery tube (V_2 is the volume of the tube downstream from the lateral inlet) and $\phi = Q_1/Q_2$ is the ratio of the flow rates injected in the two tubes, which in experiments is typically less than 1. We assume that the odorized air injected through the lateral hole at concentration c_1 mixes rapidly with the clean air stream. q is the state of the air flow through the first tube. Before the pulse, the valve upstream of the first tube is off and q=0. When the valve turns on, q rapidly increases to 1 as the air flow rapidly increases to its maximum speed. When the valve is shut off the contrary happens and q rapidly decays back to zero. Eqn 1 is linear in the concentration c_2. Thus, doubling the concentration at the input, c_1, doubles the concentration at the output c_2. Nothing in this equation depends on the identity of the odor, indicating that in the absence of interactions with surfaces, the time-dependent shape of the odor pulse delivered is independent of the identity of the odorant.

Odorant molecules may interact with the surface of the delivery tube. These interactions are used for example in the field of chromatography to separate substances within a mixture based on their retention time on the walls of a column (Deming et al., 2019; Wong et al., 1999). Similarly, we can model the loss of odorant molecules from the gas phase to the inner surface of the tube by adding an extra term to the equation:

$$\tau_2 \frac{dc_2}{dt} = \underbrace{q\phi c_1}_{\text{influx}} - \underbrace{(1-q\phi)c_2}_{\text{efflux}} - \underbrace{\tau_2 w \frac{d\theta_2}{dt}}_{\text{surface interaction}}, \quad (2)$$

where θ_2 is the fraction of the tube surface that is covered by odorant molecules and w=$2W/R_2$, where W represents the surface density of binding sites for odorant molecules. This equation must be

Journal of Experimental Biology (2019) 222, jeb207787. doi:10.1242/jeb.207787

supplemented with an additional equation that describes how θ_2 changes as a function of time:

$$\frac{d\theta_2}{dt} = k_a c_2(1-\theta_2) - k_d\theta_2. \quad (3)$$

The goal of this coarse-grain model is to provide a quantitative framework for the experimentalist to build intuition and to help with the design of simple delivery systems such as the one depicted in Fig. 1A or Fig. 3A. In this model c_2 and θ_2 represent the concentration of the odor in the gas phase and on the surface averaged over the entire tube. Likewise, k_a and k_d are the effective rates of binding and unbinding averaged over the entire tube and therefore depend on the velocity profile of the flow inside the tube (which is typically the same for all odors in a given experiment) as well as the diffusivity of odor molecules through the air (which is not).

In standard delivery systems like the one depicted in Fig. 1A, the flow is typically laminar. In Fig. 1, the air speed during an odor pulse is u_2=179 cm s^{-1} and the Reynolds number is 568. The radial profile of odor concentration in the tube homogenizes with characteristic time scale $\tau_{decay}=R_2^2/(3.8^2D)\cong 56$ ms (using D=0.073 cm^2 s^{-1} the molecular diffusion of ethyl acetate) as it is transported by a constant air flow down the delivery tube (Taylor, 1953). This decay time is on the same order as the time it takes for the air to flow from the odor injection point to the exit of the delivery tube (τ_2=50 ms). Thus, even if the odor was injected exactly at the center of the tube, it would have time to interact with the inner surface of the tube. In standard delivery systems like Fig. 1A, the injection of odor also causes a perturbation in the flow field which further helps homogenize the odor profile across the tube. Finally, on time scales longer than the decay time τ_{decay}, odor molecules experience enhanced diffusivity (Taylor's dispersion; Taylor, 1953) $D_{eff}=D(1+Pe^2/192)$, along the direction of the tube due to the shear flow in the pipe. The Peclet number $Pe=2R_2u_2/D\cong 1187$ for ethyl acetate. For tubes longer than $\tau_{decay}u_2$ ($\cong$ 10 cm in our case), this affects the temporal profile of the stimulus delivered. One way to mitigate these problems is to use a larger tube radius so that τ_{decay} becomes longer. To fully account for these effects, a model that considers the spatio-temporal dynamics of odor concentration along and across the tubes is needed, but is beyond the scope of this paper.

To understand the basic effect of surface interactions on the stimulus dynamics it is instructive to make the simplifying assumption that the odorant–surface interactions are much faster than the transport of odorant by the flow. Solving Eqn 3 at quasi-steady state and inserting in Eqn 2 yields:

$$\underbrace{\tau_2\left(1+\frac{\frac{w}{K_d}}{\left(1+\frac{c_2}{K_d}\right)^2}\right)}_{\tau_{eff}}\frac{dc_2}{dt} = q\phi c_1 - (1+q\phi)c_2 \quad (4)$$

where $K_d=k_d/k_a$. Comparing this with Eqn 1, we see that the effective timescale τ_{eff} of the stimulus kinetics now depends on several parameters of the odor-delivery system and on the odorant concentration. Eqn 4 indicates that the effect of surface interactions becomes significant when the effective concentration of surface binding sites per volume $w=2W/R_2$ becomes much larger than the dissociation constant K_d. Thus, one way to mitigate such effects is to use a tube material that is more inert therefore reducing W and increasing K_d. One can also reduce w by increasing the inner radius R_2 of the delivery tube. However, this is costly and often not practical because an increase in the radii leads to a quadratic increase in the volume of air and odor that must be flown through the delivery system. For odorants that do not interact extensively with surface, i.e. when $c_2 \ll K_d$, the denominator on the left-hand side of the equation becomes 1 and Eqn 4 becomes linear in c_2. In this case, the kinetics of odor pulse are independent of the odor concentration. Odorants that satisfy these conditions ($w \ll K_d$ or $c_2 \ll K_d$), such as ethyl acetate interacting with glass tubes, were called 'fast' odorants in Martelli et al. (2013). In contrast, for odorants that interact significantly with surfaces, i.e. when c_2 is on the same order as K_d, Eqn 4 predicts that the pulse kinetics depend on odor concentration. A possible example of such an odorant is diethyl succinate, previously called a 'slow' odorant in Martelli et al. (2013) based on its interactions with glass delivery tubes. As the odor concentration becomes smaller, the time scale τ_{eff} becomes larger.

To complete our simple model of the delivery system in Fig. 1A, we must also model the odor concentration in the gas phase, c_1, and on the surface, θ_1, of the volume used to inject the odor into the delivery tube. Similarly to Eqns 2 and 3 we have:

$$\frac{dc_1}{dt} = \frac{c_0-c_1}{\tau_s} - \frac{qc_1}{\tau_1} - \frac{w}{L/H}\frac{d\theta_1}{dt}, \quad (5)$$

$$\frac{d\theta_1}{dt} = k_a c_1(1-\theta_1) - k_d\theta_1, \quad (6)$$

where $\tau_1=\frac{V_1}{Q_1}$, $L=V_1/V_2$ and $H=A_1/A_2$ are geometric factors that depend on the relative volume and surface of the two tubes. If the radius of the tubes is the same then L/H=1. The first term on the right-hand side of Eqn 5 represents the dynamics of equilibration between the odor concentration right above the liquid source, c_0, and the gas phase concentration in the tube, c_1. The time scale, τ_s, depends on the diffusion coefficient of odorant molecules in the gas phase and the air dynamics in the head space. When using pure odorants in liquid phase and when the system was allowed to reach equilibrium, c_0 is the gas concentration at saturated vapor pressure. When odors are diluted in paraffin oil, or when multiple odorants are mixed in the liquid phase, c_0 becomes a complex function of the concentrations of odorants in the liquid phase because the presence of one compound can affect the evaporation rate of another one. These complex effects are manipulated by the perfume industry to control the timing of release of various 'notes' of a perfume (Teixeira et al., 2009).

After normalizing c_2 and c_1 with the concentration c_0, we can rewrite these equations as follows:

$$\tau_2\frac{dx_2}{dt} = q\phi x_1 - (1+q\phi)x_2 - \tau_2\tilde{w}\frac{d\theta_2}{dt}, \quad (7)$$

$$\tau_a\frac{d\theta_2}{dt} = x_2(1-\theta_2) - \tilde{K}_d\theta_2, \quad (8)$$

$$\frac{dx_1}{dt} = \frac{1-x_1}{\tau_s} - \frac{qx_1}{\tau_1} - \frac{\tilde{w}}{L/H}\frac{d\theta_1}{dt}, \quad (9)$$

$$\tau_a\frac{d\theta_1}{dt} = x_1(1-\theta_1) - \tilde{K}_d\theta_1, \quad (10)$$

where $\tilde{w}=w/c_0=A_2W/V_2c_0$ and $\tilde{K}_d=\frac{k_d}{k_a c_0}=K_d/c_0$ are now non-dimensional parameters, $\tau_a=1/k_a c_0$, and $q(t)=g(t, t_1, \sigma_1)(1-g(t, t_2, \sigma_2))$ with $g(t, s, \sigma)=1-\exp(-(t-s)/\sigma)$ when $t>s$ and zero otherwise. Here, t_1 and t_2 are the time at which the valve is turned on and off

Journal of Experimental Biology (2019) 222, jeb207787. doi:10.1242/jeb.207787

and σ_1 and σ_2 the time scale for the air to start and stop flowing, respectively.

Fitting the model to the measured data

Eqns 7–10 provide a set of 4 ordinary differential equations that describe how odorants can bind and unbind to surfaces on the two tubes and can lead to complex temporal profiles measured at the outlet. This system of equations has only four unknown parameters ($\tau_a, \tau_s, \tilde{K}_d, \tilde{w}$), and all other parameters are determined by the geometry of the system. The outflux of odorant coming out of the main tube is

$$f_2 = (1 + q\phi)x_2,$$

which is the quantity being measured. As the value of c_0 is unknown in the dataset considered here, we fitted f_2 normalized by its peak to PID measurements of the odor concentration also normalized by their maximum value.

To understand how different parameters of the model affect the shape of the odor puffs, we fitted the model to square pulses of 27 different odorants (Fig. 1 and Fig. S1).

Rapid liquid–gas phase equilibration timescale (τ_s)

For most odors, and for short odor pulses, the time it takes to replace the air in the source tube, τ_1=0.6 s, is much longer than the liquid–gas phase equilibration time scale τ_s, in which case Eqns 9 and 10 can be assumed at steady state: $x_1 \cong 1/(1+q\tau_s/\tau_1) \cong 1$ and the model reduces to the following two equations with three parameters $\tau_a, \tilde{K}_d, \tilde{w}$:

$$\tau_2 \frac{dx_2}{dt} = q\phi x_1 - (1 + q\phi)x_2 - \tau_2 \tilde{w} \frac{d\theta_2}{dt}, \quad (11)$$

$$\tau_a \frac{d\theta_2}{dt} = x_2(1 - \theta_2) - \tilde{K}_d \theta_2. \quad (12)$$

For odors that evaporate more slowly (value of τ_s closer to τ_1) and for longer pulses, the evaporation at the source might not keep up with the rate at which the air is replaced in the source tube, in which case following an initial peak the concentration of odor entering the delivery tube, x_1, will decay. In such cases, the full set of four Eqns 7–10 should be used instead. These effects can be explored using the MATLAB toolbox we provide (see below).

The limiting case of no surface interaction

Some odorants have sharp temporal profiles with rapid rise and decay times. In this case, interactions with the surface are considered to be negligible, and therefore the dynamics of the odorant are given entirely by Eqn 11, with $\tilde{w} = 0$. The kinetics of odorant pulses in this limiting case are therefore determined entirely by physical parameters of the delivery system like the flow rates and tube size, and do not depend on the odorant at all. This limiting case is used to fit the kinetics of so-called 'fast' odorants, such as ethyl acetate in Fig. 1B.

Odor-dependent surface interaction

The kinetics of most odors in our dataset could only be reproduced considering slow interactions of the odorant with the surface and could not be reproduced by simplifications of the model. To estimate the three parameter values that determine these kinetics, we fitted each odorant concentration 30 times and generated confidence intervals of parameters that fitted these data (Fig. 1C). We provide a MATLAB toolbox with interactive sliders that can be manipulated for immediate feedback and evaluation and visualization of the model (available at https://github.com/emonetlab/controlling-dynamic-stimuli). This toolbox provides a platform for the experimentalist to gain intuition about why a measured odor puff has a particular shape, and to decide how to change experimental parameters (flow rates, tube size, etc.) to change the shape of the pulse if needed.

Visualizing model fits

Overall odorants distribute in the parameter space (Fig. 1D), although they do not fill this space uniformly. For visualization, we have color coded odorants according to: $\eta = \bar{\tilde{w}} + (1 - \bar{\tau}_a) + (1 - \bar{\tilde{K}}_d)$, with the parameters normalized by their range. η approaches zero for 'fast' odorants that have slow binding (large τ_a), low affinity (large $\tilde{K}_d$) and few binding sites (low $\tilde{w}$), and is maximum for 'slow' odorants that can bind many more binding sites with larger affinity.

Odor delivery system

The odor delivery system shown in Fig. 1A and Fig. 3A is built of a few off-the-shelf components that can be reconfigured based on the task. The key ingredients are as follows: a source of pressurized air to power the system and generate flows, instruments to regulate flows (mass flow controllers, MFCs), valves to divert flows, tubing to connect different parts together, a glass tube to deliver the odorized airstream to the preparation, and a device to measure the output (a photo-ionization detector, PID). For a source of pressurized air, we used 'dry air' from Airgas (AI D300) which is purified compressed atmospheric air. Air from this pressurized cylinder was delivered to a set of MFCs (Alicat Scientific MC-series) that regulated flow to downstream components. We chose these MFCs since they can be interfaced with in a number of ways, including via USB, and provide programmable parameters of the underlying control system, allowing us to tune them to desired applications (for example, a MFC that is dedicated to maintaining a steady flow that does not change can be configured with control parameters that enhance stability at the cost of speed, while a MFC that is used for rapidly varying flow through an odorant vial to generate dynamical odorant signals can be optimized for speed of response). We used solenoid valves (Lee Co., LHDA 1231515H) to divert flows either to the preparation or to waste. Pure odorant was contained in generic 30 ml glass scintillation vials. We drilled holes in the cap and threaded them so we could fit them with push-to-connect tube fittings (McMaster Co., 1/8: tubing, 10-32 UNF 52065K211). This allowed for a modular container to hold pure odorants that could quickly be connected to the rest of the system.

To connect different components together, we used 1/8″ Teflon tubing (McMaster Carr, 5239K24) since odorants stuck to this material minimally (other common tubing materials such as soft Tygon plastic bound far more to common laboratory odorants, and should be avoided). A good test of the material being used for tubing is to deliver an odorant pulse through it, disconnect the source, and deliver another pulse. If odorants bind to the material extensively, the second control pulse will not be entirely flat. To connect tubes to each other, we used push-to-connect fittings (e.g. McMaster Carr, 5111K102, 5779K21, 5779K41).

No component is perfect, and it is important to understand the limitations of the parts being used to build an odor delivery system. Neglecting these shortcomings can lead to unanticipated and hard-to-diagnose failure modes in the assembled system. For example, for the Lee valves we used, their series resistance varied substantially from valve to valve, meaning that it was impossible to use them in parallel to build a symmetric switch. While use of Teflon tubes can minimize contamination with odorants, odorants can still adhere to

Journal of Experimental Biology (2019) 222, jeb207787. doi:10.1242/jeb.207787

the interior of tubes. To minimize contamination, we used separate tubes and connectors for each different odorant. The interior of the solenoid valves we used are not coated with Teflon, and therefore we also used a different valve for every odorant.

Software

Many of the results we present in the text were made possible by converting the problem of configuring and tuning hardware elements into a software optimization problem. This enabled parameter searches that would be otherwise prohibitively tedious. We wrote controller (available at https://github.com/emonetlab/controlling-dynamic-stimuli), a MATLAB-based data acquisition and control system that could automate many tasks. A small MATLAB toolbox that tunes the control parameters of MFCs is available at https://github.com/emonetlab/controlling-dynamic-stimuli.

Optimizing control signals iteratively to match odor statistics

Software to interactively optimize control signals to deliver naturalistic odorant signals (like in Fig. 2) is available at https://github.com/emonetlab/controlling-dynamic-stimuli, which can be used as a template to build other optimization routines. This software implements a simple online optimizer that tweaks control signals (m) to MFCs so that a desired pulse amplitude is achieved. The principle of operation is as follows: after a few iterations, data corresponding to several different MFC control signal amplitudes m_i and resultant PID measurements of the pulse y_i are fitted using a linear function $y=f(m)$. This function is then inverted to find the best estimate of the MFC control signal amplitude that yields the desired PID signal: $m_{i+1}=f^{-1}(y_0)$. The process stops when measured PID signal is within some target tolerance of the desired PID signal.

How to estimate the dose-response curve of an olfactory neuron using odorant pulses

Short pulses of odorants are usually used to estimate the dose-response curve of single neurons (Martelli et al., 2013; Cafaro, 2016; de Bruyne et al., 2001). A simple way to generate odorant pulses of varying concentrations is to force air through cartridges containing odorants diluted to varying degrees in a solvent such as paraffin oil. Fig. S2A shows a typical dose-response measured by delivering odorants using this method. The peak firing rate of the ORN ab3A varies non-linearly with the liquid phase concentration of the odorant in the cartridge and can be fitted by a Hill function. PID measurements of the stimulus intensity for every trial allow us to compare measured stimulus intensity to the nominal liquid phase concentration (Fig. S2B). Significant deviations from linearity and considerable trial-to-trial variability are evident (Fig. S2B). Moreover, plotting the response of ab3A against the measured gas phase concentration (Fig. S2C) yields different parameters from a fit with a Hill function. This suggest that the liquid phase concentration is not always an accurate proxy for the gas phase concentration and can thus bias estimations of response properties of neurons.

Most trial-to-trial variability in the stimulus is due to a slow decay in the odor concentration, as shown for four odorants at different liquid phase concentrations (Fig. S2D–H). This problem is mostly due to the depletion of the liquid dilution which depends on the volatility of the compound used (cf. ethyl acetate vs diethyl succinate) (Andersson et al., 2012) and the time τ_s necessary for the gas concentration to reach equilibrium. One way to ameliorate this problem is to use a mass flow controller (MFC) to vary the airflow through a scintillation vial containing pure odorants (Fig. S2I–M) (Gershow et al., 2012; Kim et al., 2011; Johnson et al., 2003; Bhattacharyya and Bhalla, 2016). The concentration of odorant in the odorized airstream depends only on the flow rate set by the MFC and τ_s (see steady state solution of Eqns 7 and 9), and it is stable over time as long as there is some odorant left in the vial and the air is blown continuously through it (and sent to exhaust). In this configuration, the solenoid valve is then placed downstream of the odor source. Pulses delivered using this method are more 'square' than the previous method (Fig. S2D,I), and do not show any significant decay in amplitude over 10 trials (Fig. S2J–M), even for volatile odorants like ethyl acetate. This method allows the experimenter to easily switch between different stimulus amplitudes by changing the flow rate, allowing automation of data collection.

In *Drosophila*, olfactory receptor neuron responses are invariant with air speed (Zhou and Wilson, 2012), and fluctuations in air speed caused by the method described here do not affect experiments that seek to characterize the response properties of these neurons. In applications where variations in air speed must be minimized, one can use two MFCs (one for the clean air and one for the odorized air) and adjust them simultaneously (van Breugel et al., 2018; Gupta et al., 2016 preprint).

How to deliver intermittent odorant signals

Odor cues seldom occur as isolated pulses in natural settings. Instead, they arrive in intermittent series of pulses whose statistics carry information about the odor source location (Murlis et al., 1992). Thus, various types of fluctuating odorant stimuli have been used to characterize the dynamic response properties of ORN (Martelli et al., 2013; Nagel and Wilson, 2011; Kim et al., 2011, 2015; Raiser et al., 2017). As in other sensory modalities (Chichilnisky, 2001; Baccus and Meister, 2002), paired recordings of a fluctuating sensory signal and the corresponding neural response have been used to estimate the linear kernel that best describes the transformation from the stimulus to the response (Martelli et al., 2013; Nagel and Wilson, 2011; Kim et al., 2011; Geffen et al., 2009; Schuckel and French, 2008).

The linear kernel can then be used to predict the time series of the response of that neuron to a novel stimulus that the neuron has not previously been exposed to. For example, this approach revealed that for many odor–receptor combinations in the *Drosophila melanogaster* antenna, the linear response kernels of ORNs were more invariant than previously anticipated (Martelli et al., 2013; Si et al., 2019). A favorable stimulus to use for this purpose is Gaussian white noise. Its tight autocorrelation structure allows sampling as many frequencies of the neuron response as possible. Using such a stimulus, linear filters can be estimated in an unbiased fashion, even in the presence of an output nonlinearity (Chichilnisky, 2001).

However, Gaussian white noise odorant signals are hard to realize. Interaction of the odorant with the walls of the delivery system (Martelli et al., 2013), limits on the airspeed used in the delivery system and non-infinitesimal timescales of the components of the delivery system introduce temporal correlations into every odorant stimulus. Hence, in practice, the stimulus is never 'white'. Furthermore, since the easiest way to control an odorant signal is to use a valve to divert an odorized airstream towards or away from the preparation (animal subject), early work using fluctuating odorant signals to identify linear kernels from ORN responses used binary odorant stimuli where the stimulus was either on or off (Martelli et al., 2013; Nagel and Wilson, 2011; French et al., 2014; French and Meisner, 2007; Schuckel et al., 2008, 2009) (Fig. S3A,B). This tends to generate a bimodal stimulus distribution (Fig. S3E–H), with the lower peak close to zero, and the larger peak at some value that can be controlled by the concentration of the odorized airstream

Journal of Experimental Biology (2019) 222, jeb207787. doi:10.1242/jeb.207787

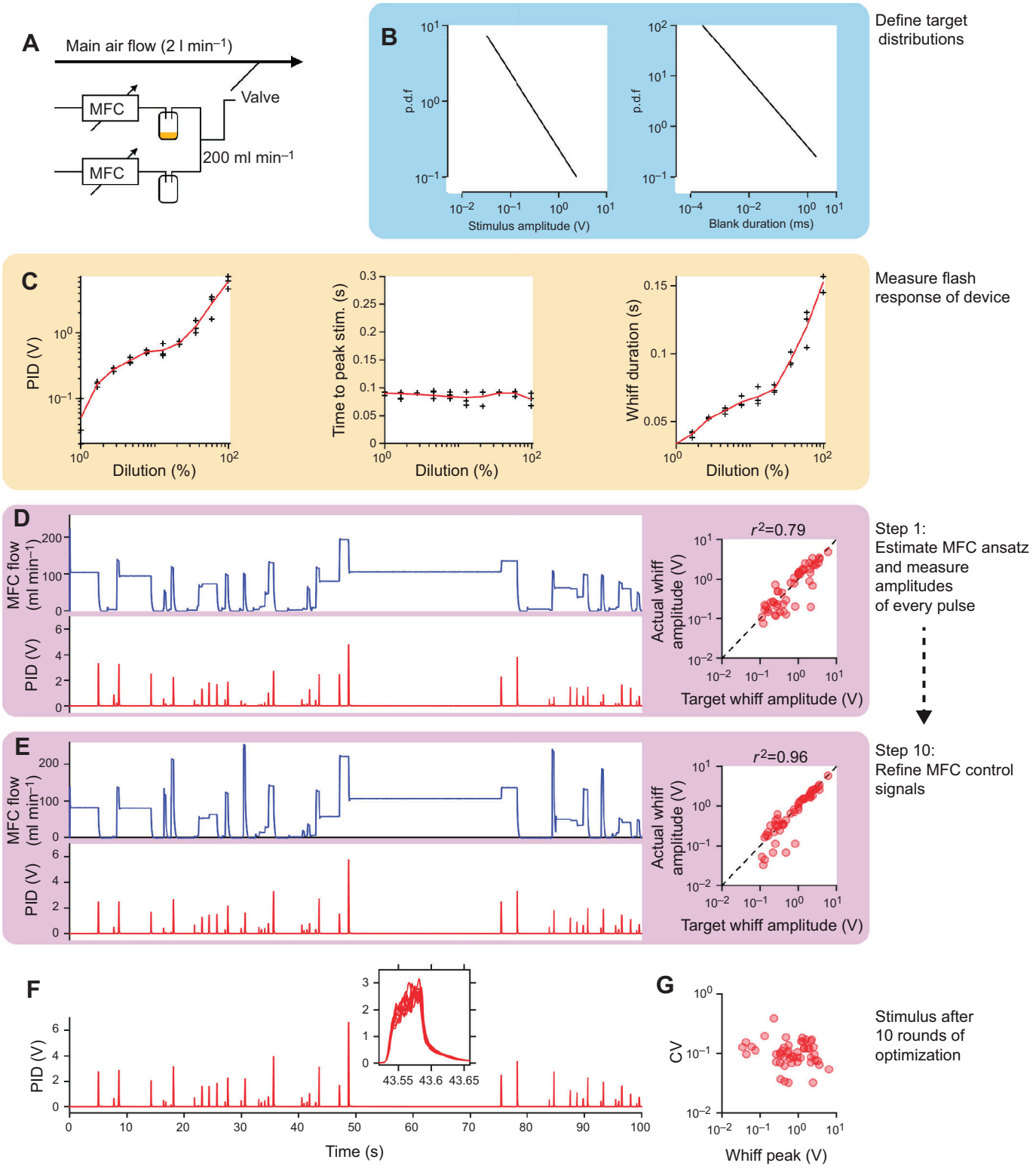

Fig. 2. How to deliver odorant stimuli with naturalistic statistics. (A) Schematic of delivery system. (B) Probability density functions (pdfs) for target whiff amplitude and blank durations. (C) Flash response of device. (D) Odorant concentration (red) in response to MFC ansatz (blue). Right panel shows correlation between measured whiff amplitudes and desired whiff amplitudes. (E) Odorant signal after ten rounds of optimization. (F) Final stimulus showing reproducibility over 10 trials (inset). (G) Coefficient of variation (CV) of whiff amplitude vs whiff peak. MFC, mass flow controller.

(Fig. S3A,B). The correlation time of the signal can be controlled by varying the switching time of the valve, and for volatile odorants that do not interact strongly with the surfaces of the delivery system, correlation times as fast as 30 ms can be realized (Martelli et al., 2013) (Fig. S3I–L). In these binary stimuli, the mean stimulus is typically rarely realized, and the responses of the neuron are dominated by responses to the large, rapid increases of odorant on valve opening (Martelli et al., 2013; Nagel and Wilson, 2011).

Journal of Experimental Biology (2019) 222, jeb207787. doi:10.1242/jeb.207787

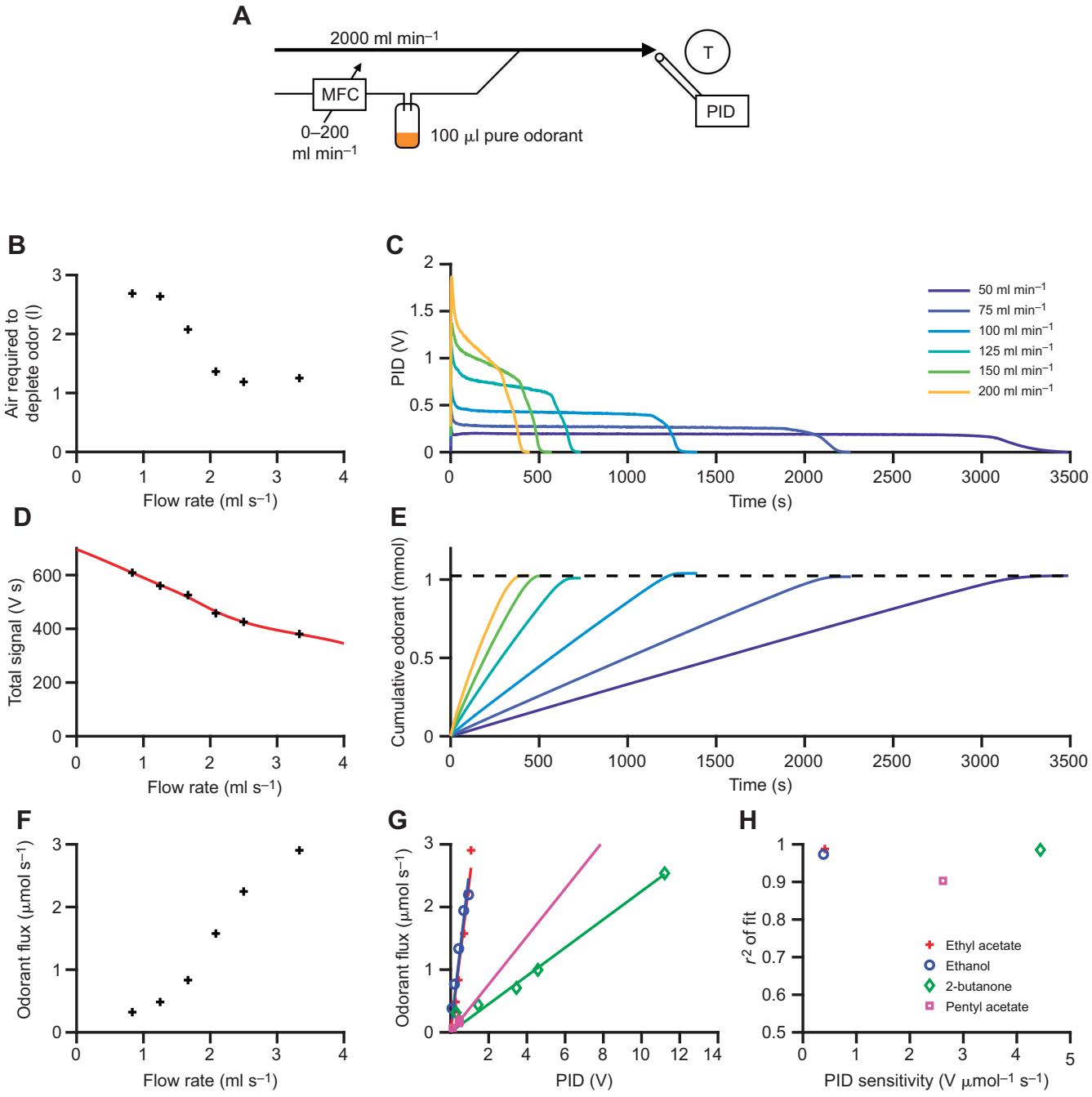

Fig. 3. How to calibrate a photo-ionization detector (PID) to any odorant it can detect. (A) Schematic for PID calibration. (B) Air required to completely deplete the odorant vs flow rate. (C) PID traces to complete depletion of odorant. (D) Integrated PID signal vs flow rate with spline interpolant (red). (E) Cumulative odorant vs time. Dashed line is at 1.02 mmol. (F) Mean odorant flux vs flow rate. (G) Odorant vs PID value, for ethyl acetate (red crosses), ethanol (blue circles), 2-butanone (green diamonds) and pentyl acetate (pink squares) fitted by a linear relationship. (H) Correlation coefficient (r^2) of fit vs PID sensitivity. MFC, mass flow controller.

An alternative approach can deliver intermittent odorant signals that have a unimodal, more Gaussian distribution. Using an MFC to vary the flow rate of an airstream through a vial of pure odorant generates an odorized airstream with a gas phase concentration that depends on the flow rate through the odorant vial (Fig. S3C,D) (Kim et al., 2011, 2015). Odorant stimuli delivered this way typically do not need to 'bottom out' at zero stimulus (Fig. S3E–H), and have mean values close to their mode. The autocorrelation time of a stimulus delivered this way is limited by the update rate of the MFC (Fig. S3I–L). If odorant stimuli with tighter autocorrelation functions are desired, multiple MFCs can be chained in parallel, driven by uncorrelated control signals (not shown).

Applicability and limitations

The methods we have described here will be useful in experiments that seek to characterize the dynamic properties of olfactory sensory periphery in immobilized animals. Potential applications include measuring the dose-response properties of olfactory neurons, characterizing their impulse response functions and

Journal of Experimental Biology (2019) 222, jeb207787. doi:10.1242/jeb.207787

measuring their adaptive properties, either as a function of controlled stimulus statistics or during naturalistic presentations of odorant.

These methods have the following limitations, which may preclude their use in other applications. In these methods, airspeed is not controlled, with airspeed either changing during periods of odor stimulation, or small transients in air flow caused by the sudden switching of valves. This means that these methods are applicable in experimental preparations where fine control of trial-to-trial odorant variability is more important than minimizing changes in airspeed. One example is the characterization of olfactory neuron responses in *Drosophila*, which have been shown to be invariant to air speed (Zhou and Wilson, 2012). In other applications, for example, in behavioral experiments, the exquisite sensitivity many animals show to changes in airflow limit the use of these techniques, and can confound results (van Breugel et al., 2018). Previous work that is complementary to this paper has focused on delivering odorants and mixtures of odorants with minimal changes in airspeed (Gupta et al., 2016 preprint; Burton et al., 2019). Furthermore, our methods are focused on delivering and measuring one odorant at a time, and delivering and measuring mixtures of odorants is beyond the scope of this work.

RESULTS AND DISCUSSION

Basic parameters that affect the kinetics of an odor pulse

A common method of delivering odorants is to create odorized air by evaporation of liquid odorant (Fig. 1A) and to push it into a main delivery tube where a constant stream of clean air is flowing. Signal intensity can be controlled by diluting the odor in liquid phase (e.g. mixing pure odor with paraffin oil) (Hallem and Carlson, 2006; Su et al., 2012; Helfand and Carlson, 1989). A valve upstream of the odorant controls odor timing. This system has been used to screen through large numbers of odorants (Mathew et al., 2013; Hallem et al., 2004) and to estimate ORN sensitivity (Mathew et al., 2013; Hallem and Carlson, 2006). Using this approach to measure the response kinetics of ORNs, in particular the linear response function of neurons, has been more challenging. PID measurements have revealed that stimuli delivered in this way typically exhibit intrinsic odorant-dependent dynamics before any interaction with the animal takes place (Martelli et al., 2013), which therefore can obscure the neural response function of ORNs.

To gain intuition about the parameters that affect odor stimulus dynamics we created a mathematical model of the delivery system (Fig. 1A, see Materials and Methods). The model includes odor transport, liquid-gas phase equilibration and surface interactions and consists of two equations with three parameters (Eqns 11,12). The first two parameters are the density of odor-binding sites on the inner surface of the tube, $\tilde{w}$, and the dissociation constant between the odor and surface, $\tilde{K}_d$. They are non-dimensional and normalized using the concentration of odor at the source. The third parameter, τ_a, is the time scale of odor to surface binding (inverse rate of binding) (see Materials and Methods). We used the model to fit PID measurements of 27 commonly used odorants delivered in 500 ms squared pulses (Martelli et al., 2013).

For six odors, surface interactions were negligible and the model could be further simplified (Fig. 1B and Materials and Methods). In this limit, the kinetics of the odorant pulse depend only on the physics of the delivery system and are independent of odorant type. However, surface interactions need to be taken into account to explain the temporal profile of most odorants in our dataset (Fig. 1C). Some of the odorants (red) can be fit with models with low affinity to the surface (high $\tilde{K}_d$) and few surface binding sites (low $\tilde{w}$). As $\tilde{w}$ increases, the pulse shape becomes rounder (red–orange). Odorants as geraniol (yellow–green), which fit with a similar τ_a, but lower $\tilde{K}_d$, show a lingering plateau after the valve turns off, indicating slow unbinding kinetics. Odors as 4-methylphenol (cyan) are fit with a lower affinity but higher $\tilde{w}$, so that their kinetics looks quite slow, but linger for a shorter time in the tube. Odorants with even slower rising phase (blue) are usually fit with fast binding kinetics (lowτ_a), which in general correlates with an increase of the plateau (low $\tilde{K}_d$). Overall, odorants distribute as a continuum in the parameter space (Fig. 1D), although they do not fill this space uniformly.

In summary, this simple model that takes into account surface interactions can reproduce complex odor-dependent kinetics of simple odor puffs routinely used in the lab. Having a quantitative framework to understand how these basic mechanisms affect odor stimuli is important for the design of odor delivery systems and the prediction of stimulus kinetics that affect response to odorants (Martelli et al., 2013) and odorant mixtures (Su et al., 2011).

Delivering odor stimuli with naturalistic and defined statistics

Sensory systems have evolved to encode naturalistic stimuli in neural signals. Using naturalistic stimuli has therefore been a powerful approach to characterize the function of sensory neurons (Cao et al., 2011; Clark et al., 2014; Simoncelli and Olshausen, 2001; Schwartz and Simoncelli, 2001; Rieke and Rudd, 2009). This approach is more challenging in olfaction, because natural odor signals are comprised of whiffs and 'blanks' whose intensities and durations can be distributed over many orders of magnitude (Murlis et al., 1992, 2000; Celani et al., 2014). Using naturalistic odorant stimuli could reveal features of neuron coding not readily apparent from studying responses to artificial odorant signals. Previous efforts have used a fan to drive air over an odor source, mimicking natural plumes, but the resulting stimulus pattern is not reproducible (Martelli et al., 2013; Budick and Dickinson, 2006; Nagel and Wilson, 2011; Vickers et al., 2001), ruling out estimating neural responses by trial averaging.

Our approach is to deliver an odorant signal whose whiff and blank statistics are drawn from a known distribution. We exploited the fact that some naturalistic signals can be approximately segmented into short pulses. Therefore, a target signal can be approximated by adjusting the amplitude, duration and intermittency of a set of single whiffs. The experimental apparatus we used is shown in Fig. 2A. A pair of MFCs regulate airflow through an odor vial, controlling odor concentration. A valve enables pulse timing control. Thus, MFC and valve control signals can be iteratively tuned until the measured signal is sufficiently close to the target signal.

First, we defined target distributions of whiff intensity and the durations between whiffs (Fig. 2B). We characterized the flash response of the odor delivery system, which determines the control signals to the MFC and valve needed to generate a pulse of a desired amplitude. Setting MFC flow rates to some fixed value, we briefly activated the valve, and measured the resultant PID waveform. By repeating this procedure over multiple MFC flow rates, we can fit functions that approximately describe how the pulse statistics depend on the dilution (Fig. 2C). We then generated a target stimulus time series by repeatedly sampling from the distributions in Fig. 2B. We first sampled a whiff intensity, then drew another sample from the blank duration distribution, and so on, until a skeleton of the odor stimulus was created. Since we sampled from the target distribution in Fig. 2B, these statistics match the target distributions.

Next, we built an initial approximate control signal, or 'ansatz' for the MFC and for activation of the valves, by inverting the functions fitted in Fig. 2C. This ansatz is shown in Fig. 2D (blue trace). Measuring the stimulus using the ansatz revealed a sequence of whiffs with varying amplitudes, but their amplitudes were not perfectly correlated (r^2=0.79) with desired whiff amplitudes (Fig. 2E). These deviations stem from the fact that mapping in Fig. 2C assumed isolated flashes, which is not true in this stimulus. We therefore built a simple optimizer that varies the set point of the MFCs before each valve opening till the correlation between measured whiff intensities and desired whiff intensities is within acceptable limits. Ten rounds of this optimization increased the correlation (r^2=0.96) (Fig. 2E).

Once a desired accuracy has been reached, the stimulus can be replayed without further fine-tuning. Fig. 2F shows 10 repetitions of the same stimulus, showing high reproducibility despite the nearly 1000-fold variation in signal intensity across whiffs. The coefficient of variability (CV) for each whiff was well controlled and was independent of whiff intensity (Fig. 2G).

Calibrating PIDs

PIDs have become common tools to measure odorant stimuli, since they are fast and easy to use. However, they do not report an absolute value of the gas phase concentration of odorants. Calibration is necessary to compare the sensitivity of a receptor to different odorants (Andersson et al., 2012), or to compare stimuli, and responses across laboratories.

The PID can be calibrated using another device that can measure absolute concentrations, such as GCMS devices or flame ionization detectors (Andersson et al., 2012; Cometto-Muñiz et al., 2003). However, this shifts the problem of calibration to another system, which in turn needs to be calibrated. Another approach is to assume the odorant headspace in the device is saturated, and use Raoult's Law and Henry's Law to estimate the gas phase concentration of the odorant, and then extrapolate to fast changes reported by the PID. Such an approach has been used in Olsson et al. (2011) and van Breugel and Dickinson (2014) or in conjunction with a tracer gas of known concentration (Kim et al., 2011, 2015; French et al., 2014; French and Meisner, 2007).

Here, we propose a method to calibrate the PID to any odorant that it can detect. This method does not require additional equipment nor does it make assumptions about headspace saturation. It works by depleting a known volume of odorant and integrating the total PID signal. Since the number of molecules in the pure odorant sample can be estimated precisely using micropipettes and published datasheets, the PID signal can be mapped onto the molecular efflux rate.

For example, to calibrate the PID to ethyl acetate, we placed 100 µl of odorant in a 30 ml scintillation vial downstream of an MFC, as shown in Fig. 3A. We forced air through the scintillation vial until all odorant was depleted and repeated this for a few flow rates. The volume of air and time required to evaporate all odorant decreased with the flow rate (Fig. 3B,C). If the PID captured and ionized all odorant molecules, the integrated PID signal would be constant, corresponding to the total number of molecules of odorant in the vial. However, we observed that the total integrated PID signal decreased with the flow rate (Fig. 3D); an effect we attributed to flow-rate-dependent partial capture of odorant molecules. To compensate for this, we fitted an interpolant to this data (Fig. 3D, red line), and used this to correct for variations in the total signal. Integrating the corrected PID curves yielded curves of cumulative odorant vs time that reached approximately the same height, corresponding to the calculated number of moles of odorant (dashed line, Fig. 3E).

We then computed the odorant flux as a function of the flow rate, by estimating the slope of the cumulative odorant curves (Fig. 3F). Finally, we can combine these measurements to plot odorant flux vs the PID signal, to generate a function that maps PID values onto odorant flux. We repeated this calibration process for three other odorants (ethanol, 2-butanone and pentyl acetate), and found that all curves are approximately linear (Fig. 3G,I).

Two odor environments

Odor fluctuations are caused by moving air and therefore can carry information about the location and distance of an odor source (Murlis et al., 1992; Mafra-Neto and Cardé, 1994). How animals extract and exploit this information in different environments remains unclear. Away from surfaces, odor transport is linear, suggesting that air flow can maintain correlations between odor components, and therefore the identity of the odor. However, surface interactions can introduce delays in stimulus dynamics that are odorant specific. Thus, in the presence of surfaces individual monomolecular components of an odor might experience different delays, affecting odor identity recognition (Stierle et al., 2013; Szyszka et al., 2012). Effectively, there are two different odor environments: (1) close to surfaces, where odors might become decomposed, and (2) far from them, where odor coherence is maintained. To what extent animals are aware of this difference when interpreting odor signals remains unclear.

A better understanding and control of odor stimulation in the lab is therefore necessary. Here, we have introduced a model of odor–surface interaction (Fig. 1), which is often neglected in the interpretation of both physiological and behavioral experiments. These unavoidable interactions may be a stimulus feature that can be exploited by animals. Our model will allow for the design of experiments aimed at understanding how chemically complex odor signals are encoded in neural activity and what information is available to animals in different olfactory environments. Finally, our approach to generate and quantify temporally complex stimuli (Figs 2, 3) provides a flexible tool for the design of more quantitative experiments aimed at understanding odor coding and behavior in natural conditions.

Acknowledgements

C.M. is thankful to members of the Galizia lab for useful comments.

Competing interests

The authors declare no competing or financial interests.

Author contributions

Conceptualization: S.G.-S., C.M., M.D., T.E.; Methodology: S.G.-S., C.M., M.D.; Software: S.G.-S.; Validation: S.G.-S.; Formal analysis: T.E.; Investigation: S.G.-S., M.D.; Resources: T.E.; Data curation: S.G.-S.; Writing - original draft: S.G.-S., C.M.; Writing - review & editing: S.G.-S., C.M., M.D., T.E.; Visualization: S.G.-S., C.M.; Supervision: T.E.; Project administration: T.E.; Funding acquisition: T.E.

Funding

This research was funded by the Paul G. Allen Family Foundation (grant no. 11562). T.E. was supported by the National Institute of General Medical Sciences (R01GM106189). Deposited in PMC for release after 12 months.

Data availability

Data, code to reproduce the figures presented here, and a toolbox with interactive sliders than can be manipulated for immediate feedback and evaluation of the model are available at https://github.com/emonetlab/controlling-dynamic-stimuli.

Supplementary information

Supplementary information available online at http://jeb.biologists.org/lookup/doi/10.1242/jeb.207787.supplemental

References

Andersson, M. N., Schlyter, F., Hill, S. R. and Dekker, T. (2012). What reaches the antenna? How to calibrate odor flux and ligand-receptor affinities. *Chem. Senses* **37**, 403-420. doi:10.1093/chemse/bjs009

Baccus, S. A. and Meister, M. (2002). Fast and slow contrast adaptation in retinal circuitry. *Neuron* **36**, 909-919. doi:10.1016/S0896-6273(02)01050-4

Bhattacharyya, U. and Bhalla, U. S. (2016). Robust and rapid air-borne odor tracking without casting. *eNeuro* **2**, ENEURO.0102-15.2015. doi:10.1523/ENEURO.0102-15.2015

Budick, S. A. and Dickinson, M. H. (2006). Free-flight responses of Drosophila melanogaster to attractive odors. *J. Exp. Biol.* **209**, 3001-3017. doi:10.1242/jeb.02305

Burton, S. D., Wipfel, M., Guo, M., Eiting, T. P. and Wachowiak, M. (2019). A novel olfactometer for efficient and flexible odorant delivery. *Chem. Senses* **44**, 173-188. doi:10.1093/chemse/bjz005

Cafaro, J. (2016). Multiple sites of adaptation lead to contrast encoding in the Drosophila olfactory system. *Physiol. Rep.* **4**, e12762. doi:10.14814/phy2.12762

Cao, X., Merwine, D. K. and Grzywacz, N. M. (2011). Dependence of the retinal Ganglion cell's responses on local textures of natural scenes. *J. Vis.* **11**, 11-11. doi:10.1167/11.6.11

Celani, A., Villermaux, E. and Vergassola, M. (2014). Odor landscapes in turbulent environments. *Phys. Rev. X* **4**, 041015. doi:10.1103/PhysRevX.4.041015

Chichilnisky, E. J. (2001). A simple white noise analysis of neuronal light responses. *Network* **12**, 199-213. doi:10.1080/713663221

Clark, D. A., Fitzgerald, J. E., Ales, J. M., Gohl, D. M., Silies, M. A., Norcia, A. M. and Clandinin, T. R. (2014). Flies and humans share a motion estimation strategy that exploits natural scene statistics. *Nature* **17**, 296-303. doi:10.1038/nn.3600

Cometto-Muñiz, J. E., Cain, W. S. and Abraham, M. H. (2003). Quantification of chemical vapors in chemosensory research. *Chem. Senses* **28**, 467-477. doi:10.1093/chemse/28.6.467

Davies, A., Louis, M. and Webb, B. (2015). A model of Drosophila larva chemotaxis. *PLoS Comp. Biol.* **11**, e1004606. doi:10.1371/journal.pcbi.1004606

De Bruyne, M., Foster, K. and Carlson, J. R. (2001). Odor coding in the Drosophila antenna. *Neuron* **30**, 537-552. doi:10.1016/S0896-6273(01)00289-6

de Ruyter van Steveninck, R. and Bialek, W. (1988). Real-time performance of a movement-sensitive neuron in the blowfly visual system: coding and information transfer in short spike sequences. *Proc. R. Soc. Lond. B* **234**. doi:10.1098/rspb.1988.0055

Deming, B. L., Pagonis, D., Liu, X., Day, D. A., Talukdar, R., Krechmer, J. E., De Gouw, J. A., Jimenez, J. L. and Ziemann, P. J. (2019). Measurements of delays of gas-phase compounds in a wide variety of tubing materials due to gas–wall interactions. *Atmos. Meas. Tech.* **12**, 3453-3461. doi:10.5194/amt-12-3453-2019

Fishilevich, E., Domingos, A. I., Asahina, K., Naef, F., Vosshall, L. B. and Louis, M. (2005). Chemotaxis behavior mediated by single larval olfactory neurons in Drosophila. *Curr. Biol.* **15**, 2086-2096. doi:10.1016/j.cub.2005.11.016

French, A. S. and Meisner, S. (2007). A new method for wide frequency range dynamic olfactory stimulation and characterization. *Chem. Senses* **32**, 681-688. doi:10.1093/chemse/bjm035

French, A. S., Meisner, S., Su, C.-Y. and Torkkeli, P. H. (2014). Carbon dioxide and fruit odor transduction in Drosophila olfactory neurons. What controls their dynamic properties? *PLoS ONE* **9**, e86347. doi:10.1371/journal.pone.0086347

Frye, M. A. and Dickinson, M. H. (2004). Motor output reflects the linear superposition of visual and olfactory inputs in Drosophila. *J. Exp. Biol.* **207**, 123-131. doi:10.1242/jeb.00725

Gaudry, Q., Hong, E. J., Kain, J., De Bivort, B. L. and Wilson, R. I. (2013). Asymmetric neurotransmitter release enables rapid odour lateralization in Drosophila. *Nature* **493**, 424-428. doi:10.1038/nature11747

Geffen, M. N., Broome, B. M., Laurent, G. and Meister, M. (2009). Neural encoding of rapidly fluctuating odors. *Neuron* **61**, 570-586. doi:10.1016/j.neuron.2009.01.021

Gepner, R., Skanata, M. M., Bernat, N. M., Kaplow, M. and Gershow, M. (2015). Computations underlying Drosophila photo-taxis, odor-taxis, and multi-sensory integration. *eLife* **4**, e06229. doi:10.7554/eLife.06229.001

Gershow, M., Berck, M., Mathew, D., Luo, L., Kane, E. A., Carlson, J. R. and Samuel, A. D. T. (2012). Controlling airborne cues to study small animal navigation. *Nat. Methods* **9**, 290-296. doi:10.1038/nmeth.1853

Gomez-Marin, A., Stephens, G. J. and Louis, M. (2011). Active sampling and decision making in Drosophila chemotaxis. *Nature* **2**, 441. doi:10.1038/ncomms1455

Gupta, P., Albeanu, D. F. and Bhalla, U. S. (2016). An odor delivery system for arbitrary time-varying patterns of odors, mixtures and concentrations. *bioRxiv*. doi:10.1101/077875

Hallem, E. A. and Carlson, J. R. (2006). Coding of odors by a receptor repertoire. *Cell* **125**, 143-160. doi:10.1016/j.cell.2006.01.050

Hallem, E. A., Ho, M. G. and Carlson, J. R. (2004). The molecular basis of odor coding in the Drosophila antenna. *Cell* **117**, 965-979. doi:10.1016/j.cell.2004.05.012

Helfand, S. L. and Carlson, J. R. (1989). Isolation and characterization of an olfactory mutant in Drosophila with a chemically specific defect. *Proc. Natl. Acad. Sci. USA* **86**, 2908-2912. doi:10.1073/pnas.86.8.2908

Hernandez-Nunez, L., Belina, J., Klein, M., Si, G., Claus, L., Carlson, J. R. and Samuel, A. D. T. (2015). Reverse-correlation analysis of navigation dynamics in Drosophila larva using optogenetics. *eLife* **4**, 9. doi:10.7554/eLife.06225

Hudspeth, A. J. (2014). Integrating the active process of hair cells with cochlear function. *Nat. Rev. Neurosci.* **15**, 600-614. doi:10.1038/nrn3786

Johnson, B. N., Mainland, J. D. and Sobel, N. (2003). Rapid olfactory processing implicates subcortical control of an olfactomotor system. *J. Neurophysiol.* **90**, 1084-1094. doi:10.1152/jn.00115.2003

Kato, S., Xu, Y., Cho, C. E., Abbott, L. F. and Bargmann, C. I. (2014). Temporal responses of C. elegans chemosensory neurons are preserved in behavioral dynamics. *Neuron* **81**, 616-628. doi:10.1016/j.neuron.2013.11.020

Kim, A. J., Lazar, A. A. and Slutskiy, Y. B. (2011). System identification of Drosophila olfactory sensory neurons. *J. Comput. Neurosci.* **30**, 143-161. doi:10.1007/s10827-010-0265-0

Kim, A. J., Lazar, A. A. and Slutskiy, Y. B. (2015). Projection neurons in Drosophila antennal lobes signal the acceleration of odor concentrations. *eLife* **4**, e06651. doi:10.7554/eLife.06651.001

Klein, M., Krivov, S. V., Ferrer, A. J., Luo, L., Samuel, A. D. T. and Karplus, M. (2017). Exploratory search during directed navigation in C. elegans and Drosophila larva. *eLife* **6**, e30503. doi:10.7554/eLife.30503

Laughlin, S. B. (1989). The role of sensory adaptation in the retina. *J. Exp. Biol.* **146**, 39-62.

Mafra-Neto, A. and Cardé, R. T. (1994). Fine-scale structure of pheromone plumes modulates upwind orientation of flying moths. *Nature* **369**, 142-144. doi:10.1038/369142a0

Martelli, C., Carlson, J. R. and Emonet, T. (2013). Intensity invariant dynamics and odor-specific latencies in olfactory receptor neuron response. *J. Neurosci.* **33**, 6285-6297. doi:10.1523/JNEUROSCI.0426-12.2013

Mathew, D., Martelli, C., Kelley-Swift, E., Brusalis, C., Gershow, M., Samuel, A. D. T., Emonet, T. and Carlson, J. R. (2013). Functional diversity among sensory receptors in a Drosophila olfactory circuit. *Proc. Natl. Acad. Sci. USA* **110**, E2134-E2143. doi:10.1073/pnas.1306976110

Murlis, J. and Jones, C. D. (1981). Fine-scale structure of odour plumes in relation to insect orientation to distant pheromone and other attractant sources. *Physiol. Entomol.* **6**, 71-86. doi:10.1111/j.1365-3032.1981.tb00262.x

Murlis, J., Elkinton, J. S. and Cardé, R. T. (1992). Odor plumes and how insects use them. *Annu. Rev. Entomol.* **37**, 505-532. doi:10.1146/annurev.en.37.010192.002445

Murlis, J., Willis, M. A. and Cardé, R. T. (2000). Spatial and temporal structures of pheromone plumes in fields and forests. *Physiol. Entomol.* **25**, 211-222. doi:10.1046/j.1365-3032.2000.00176.x

Nagel, K. I. and Wilson, R. I. (2011). Biophysical mechanisms underlying olfactory receptor neuron dynamics. *Nat. Neuro* **14**, 208-216. doi:10.1038/nn.2725

Olsson, S. B., Kuebler, L. S., Veit, D., Steck, K., Schmidt, A., Knaden, M. and Hansson, B. S. (2011). A novel multicomponent stimulus device for use in olfactory experiments. *J. Neurosci. Methods* **195**, 1-9. doi:10.1016/j.jneumeth.2010.09.020

Raiser, G., Galizia, C. G. and Szyszka, P. (2017). A high-bandwidth dual-channel olfactory stimulator for studying temporal sensitivity of olfactory processing. *Chem. Senses* **42**, 141-151. doi:10.1093/chemse/bjw114

Rieke, F. and Rudd, M. E. (2009). The challenges natural images pose for visual adaptation. *Neuron* **64**, 605-616. doi:10.1016/j.neuron.2009.11.028

Riffell, J. A., Abrell, L. and Hildebrand, J. G. (2008). Physical processes and real-time chemical measurement of the insect olfactory environment. *J. Chem. Ecol.* **34**, 837-853. doi:10.1007/s10886-008-9490-7

Riffell, J. A., Lei, H. and Hildebrand, J. G. (2009). Neural correlates of behavior in the moth Manduca sexta in response to complex odors. *Proc. Natl. Acad. Sci. USA* **106**, 19219-19226. doi:10.1073/pnas.0910592106

Schuckel, J. and French, A. S. (2008). A digital sequence method of dynamic olfactory characterization. *J. Neurosci. Methods* **171**, 98-103. doi:10.1016/j.jneumeth.2008.02.013

Schuckel, J., Meisner, S., Torkkeli, P. H. and French, A. S. (2008). Dynamic properties of Drosophila olfactory electroantennograms. *J. Comp. Physiol.* **194**, 483-489. doi:10.1007/s00359-008-0322-6

Schuckel, J., Torkkeli, P. H. and French, A. S. (2009). Two Interacting Olfactory Transduction Mechanisms Have Linked Polarities and Dynamics in Drosophila melanogaster Antennal Basiconic Sensilla Neurons. *J. Neurophys* **102**, 214-223. doi:10.1152/jn.00162.2009

Schwartz, O. and Simoncelli, E. P. (2001). Natural signal statistics and sensory gain control. *Nat. Neuro* **4**, 819-825. doi:10.1038/90526

Si, G., Kanwal, J. K., Hu, Y., Tabone, C. J., Baron, J., Berck, M., Vignoud, G. and Samuel, A. D. T. (2019). Structured odorant response patterns across a complete olfactory receptor neuron population. *Neuron* **101**, 950-962.e7. doi:10.1016/j.neuron.2018.12.030

Simoncelli, E. P. and Olshausen, B. A. (2001). Natural image statistics and neural representation. *Annu. Rev. Neurosci.* **24**, 1193-1216. doi:10.1146/annurev.neuro.24.1.1193

Smirnakis, S. M., Berry, M. J., Warland, D. K., Bialek, W. and Meister, M. (1997). Adaptation of retinal processing to image contrast and spatial scale. *Nature* **386**, 69-73. doi:10.1038/386069a0

Stierle, J. S., Galizia, C. G. and Szyszka, P. (2013). Millisecond stimulus onset-asynchrony enhances information about components in an odor mixture. *J. Neurosci* **33**, 6060-6069. doi:10.1523/JNEUROSCI.5838-12.2013

Su, C.-Y., Martelli, C., Emonet, T. and Carlson, J. R. (2011). Temporal coding of odor mixtures in an olfactory receptor neuron. *Proc. Natl. Acad. Sci. USA* **108**, 5075-5080. doi:10.1073/pnas.1100369108

Su, C.-Y., Menuz, K., Reisert, J. and Carlson, J. R. (2012). Non-synaptic inhibition between grouped neurons in an olfactory circuit. *Nature* **492**, 66-71. doi:10.1038/nature11712

Szyszka, P., Stierle, J. S., Biergans, S. and Galizia, C. G. (2012). The speed of smell: odor-object segregation within milliseconds. *PLoS ONE* **7**, e36096. doi:10.1371/journal.pone.0036096.g001

Taylor, G. (1953). Dispersion of soluble matter in solvent flowing slowly through a tube. *Proc. R. Soc. Lond. A* **219**, 186-203. doi:10.1098/rspa.1953.0139

Teixeira, M. A., Rodríguez, O., Mata, V. G. and Rodrigues, A. E. (2009). The diffusion of perfume mixtures and the odor performance. *Chem. Eng. Sci.* **64**, 2570-2589. doi:10.1016/j.ces.2009.01.064

Thoma, M., Hansson, B. S. and Knaden, M. (2014). Compound valence is conserved in binary odor mixtures in Drosophila melanogaster. *J. Exp. Biol.* **217**, 3645-3655. doi:10.1242/jeb.106591

Van Breugel, F. and Dickinson, M. H. (2014). Plume-tracking behavior of flying drosophila emerges from a set of distinct sensory-motor reflexes. *Curr. Biol.* **24**, 274-286. doi:10.1016/j.cub.2013.12.023

Van Breugel, F., Huda, A. and Dickinson, M. H. (2018). Distinct activity-gated pathways mediate attraction and aversion to CO2 in Drosophila. *Nature* **564**, 420-424. doi:10.1038/s41586-018-0732-8

Vickers, N. J., Christensen, T. A., Baker, T. C. and Hildebrand, J. G. (2001). Odour-plume dynamics influence the brain's olfactory code. *Nature* **410**, 466-470. doi:10.1038/35068559

Wong, C. C., Adkins, D. R., Frye-Mason, G. C., Hudson, M. L., Kottenstette, R. J., Matzke, C. M., Shadid, J. N. and Salinger, A. G. (1999). Modeling transport in gas chromatography columns for the micro-ChemLab. *Proc. SPIE* **3877**, 120-129. doi:10.1117/12.359329

Zhou, Y. and Wilson, R. I. (2012). Transduction in Drosophila olfactory receptor neurons is invariant to air speed. *J. Neurophys* **108**, 2051-2059. doi:10.1152/jn.01146.2011

SUPPLEMENTARY MATERIAL

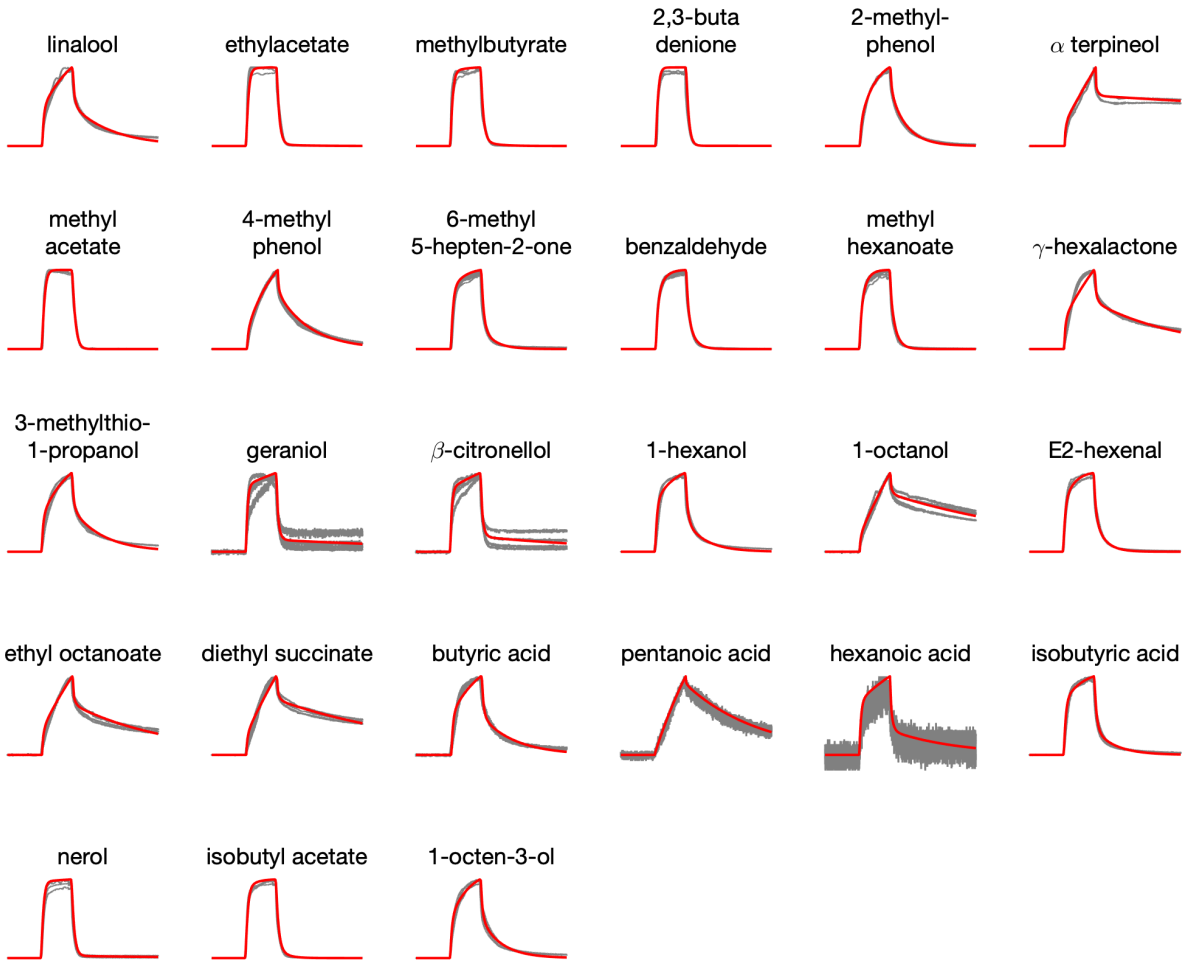

Figure S1. Diversity of odor pulse kinetics can be reproduced by a model of odorant interaction to surfaces. In each panel, gray traces show five trials of PID measurements of a 500ms pulse of that odorant. Red traces are predictions of the model (**Equations 11-12**) fit to this data. Parameters of model fits are shown in **Fig. 1**.

Journal of Experimental Biology • Supplementary information

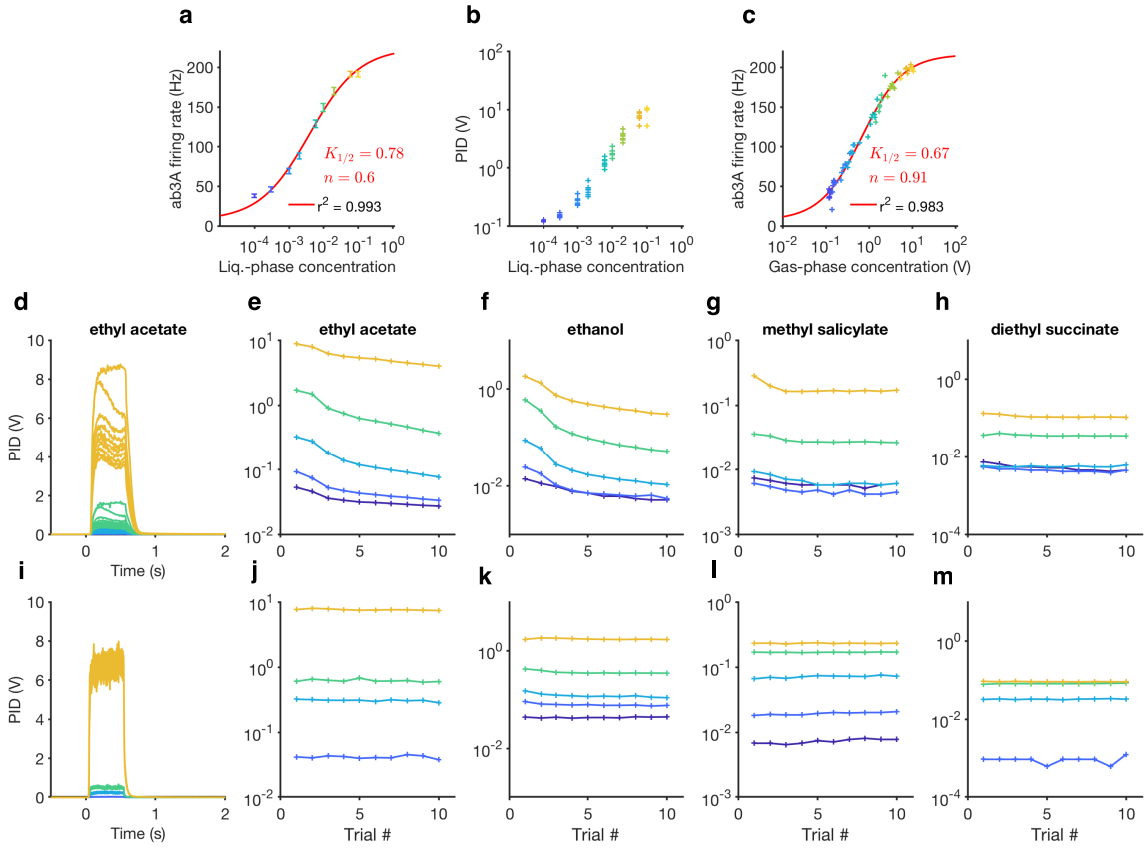

Figure S2: Gas-phase dilution enables steady delivery of short odorant pulses. **(a)** Peak firing rate of ab3A ORNs as a function of liquid-phase dilution of ethyl acetate odorant in paraffin oil in "cartridges". The red line is a best-fit Hill function. **(b)** Measured pulse amplitude *vs.* liquid phase concentration shows trial-to-trial variability and nonlinearity of measured gas phase concentration. **(c)** Peak firing rate of ab3A ORNs replotted vs. measured gas-phase concentration for every pulse. The red line is a best-fit Hill function. Note that the best-fit parameters are different in **(a)** and **(c)**. **(d-h)** 500 ms pulses of odorant delivered using liquid phase dilution. **(d)** Measured stimulus *vs.* time for different values of liquid-phase dilution of ethyl acetate. **(e-h)** Maximum pulse amplitude *vs.* trial for four different odorants. **(i-m)** 500 ms pulses of the same odorants delivered using gas-phase dilution.

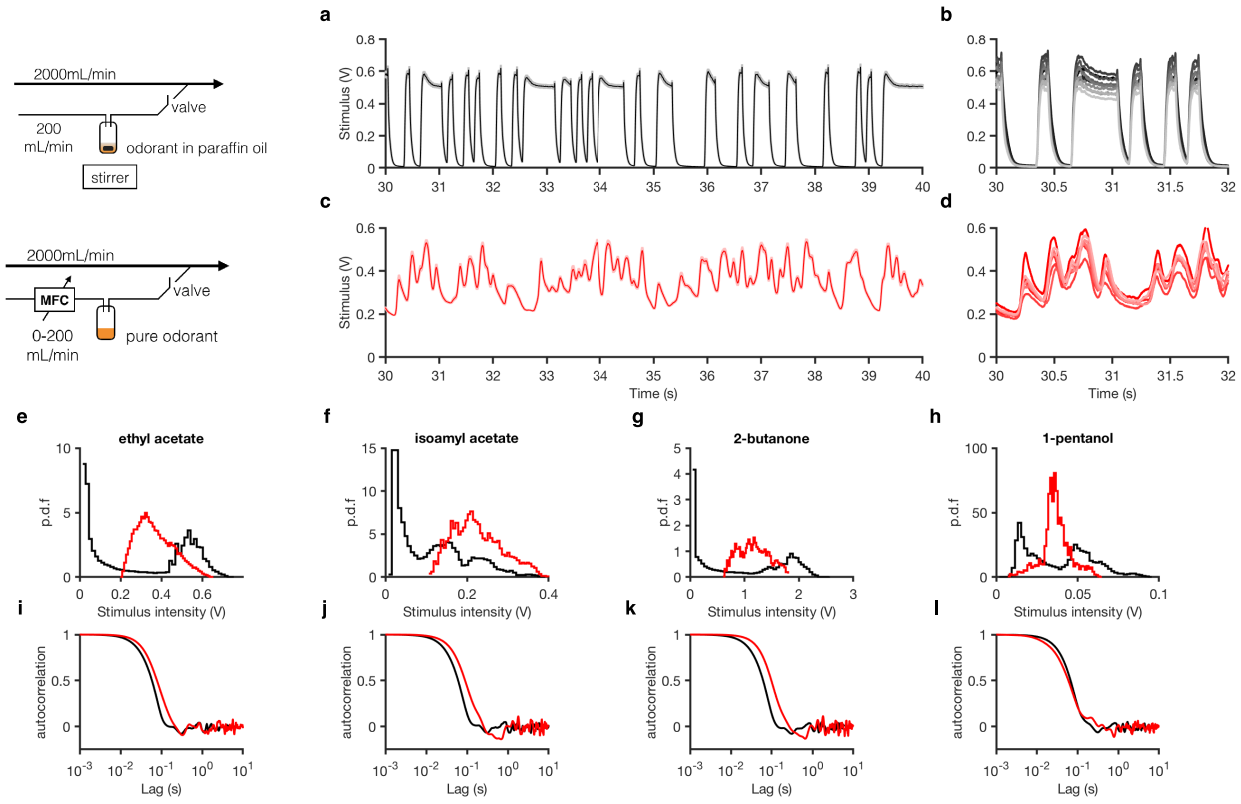

Figure S3. How to deliver intermittent odorant signals. (a-b) Using a valve to generate binary random stimuli using ethyl acetate odorant. When the valve is turned on, the odor signal tends to its maximum value, and when the valve is off, it tends to 0. **(a)** Mean ethyl acetate concentration (shading is standard error of mean). **(b)** Individual traces. **(c-d)** Using a MFC to deliver ethyl acetate with fluctuations around a desired mean. Here, the MFC is used to modulate airflow through the odorant vial, leading to fluctuations in the odor concentration. The valve is used only to shut down the airstream at the end of the odor stimulus. **(c)** Mean ethyl acetate concentration (shading is standard error of mean). **(d)** Individual traces. **(e-l)** Distributions and autocorrelation functions of stimulus time series for various odorants. Black traces are delivered using the apparatus in (a-b) and red traces are delivered using the apparatus in (c-d).